Thallium-201 Myocardial Tomography with a Rotating Slant-Hole Collimator and a Large Number of Projections

Susanne Dale and Dianna Bone

Department of Medical Engineering, Karolinska Institute, Huddinge, Sweden and Department of Clinical Physiology, Thoracic Clinics, Karolinska Hospital, Stockholm, Sweden

Tomographic imaging of the myocardium was performed using a gamma camera and a 30-degree rotating slant-hole collimator to register 64 projections from a restricted-view angle. Section images were reconstructed with a two-dimensional filtered backprojection technique. Performance in terms of resolution, effects of misalignment, and three-dimensional activity distribution was evaluated in phantom studies. In a limited clinical study, ten consecutive patients were imaged both with single-photon emission computed tomography (SPECT) and the method described. In the new method, the camera was orientated in the 30° left anterior oblique position with 15° cranial tilt. Due to the short distance from the myocardium to the camera, resolution within reconstructed section images was high, the noise level was comparatively low, and the mean activity level in the posterior wall was significantly higher ($p < 0.005$) than in SPECT.

J Nucl Med 1990; 31:1682–1687

Myocardial perfusion can be visualized by thallium-201 (^{201}Tl) scintigraphy for detection of ischemic heart disease and infarction. Both planar and tomographic imaging with a gamma camera are established techniques (*1*). Several kinds of tomography have been applied. Single-photon emission computed tomography (SPECT) (*2–4*) is theoretically superior, but coded aperture techniques (*5,6*), multiple pinhole (*7–9*), and rotating slant-hole (RSH) methods (*10–12*) have practical advantages.

With a gamma camera and a RSH collimator, the distance between myocardium and camera is small compared to SPECT. A principally new tomographic method has been implemented on such a system using a large number of projections (typically 64) and a two-dimensional filtered backprojection technique (*13–16*). Filtration consists of a high-pass filtration to reduce out-of-section activity and a low-pass filtration to define section thickness. High-pass filtration requires about 60 projections to work properly.

In systems using a restricted-view angle, the Fourier coefficients of the projections are generally incomplete when compared to those required to perform a correct reconstruction (*17,18*). Missing coefficients in the Fourier domain impose limitations on restricted-view angle methods since artifacts can be present in the reconstructed sections. In myocardial imaging, misspositioning or misalignment arises if the long-axis of the left ventricle deviates significantly from the axis of symmetry for data sampling, i.e., the axis of rotation (*9,11–13,18–28*).

The purpose of this study was to evaluate the tomographic method described using a RSH collimator and a large number of projections for ^{201}Tl myocardial imaging. Phantom studies were performed to investigate resolution with ^{201}Tl, effects of misalignment, and three-dimensional activity distribution. Comparison with SPECT was also made in a limited clinical study.

MATERIALS AND METHODS

Imaging Conditions

Studies were performed on a gamma camera with a 39-cm field of view (Maxicamera 400T, GE Medical Systems, Milwaukee, WI) connected on-line to a computer system. A low-energy general-purpose RSH collimator (Edc/Septa, Engineering Dynamics Corporation, Lowell, MA) with a slant angle of 30° was used. The collimator was rotated manually through 64 positions with an estimated maximum error of ±0.5°. For both methods, acquisition matrix size was 64 × 64 pixels.

For SPECT, routine procedures of the department of clinical physiology, Karolinksa Hospital, were followed and acquisitions were performed on the same gamma camera system using a low-energy high-sensitivity collimator (GE Medical Systems, Milwaukee, WI).

Section images parallel to the collimator face were reconstructed using the algorithm described above (commercial software will soon be available, Nuclear Diagnostic Co. Ltd.,

Received Apr. 17, 1990; revision accepted Mar. 27, 1990.

For reprints contact: Susanne Dale, PhD, Department of Medical Engineering, F60, Karolinska Institute, Novum, Huddinge University Hospital, S-14186 Huddinge, Sweden.

Stockholm, Sweden). For phantom measurements, the Shepp-Logan high-pass filter (*29*) was used and data from patient studies were processed using a Hanning-weighted ramp filter (*30*). Attenuation correction (*13*) was applied to left ventricular phantom and patient studies.

SPECT reconstructions were performed with commercially available software (SPETS V06-TSX, Nuclear Diagnostic Co. Ltd., Stockholm, Sweden). Following clinical practice, a modified form of the Shepp-Logan filter (*29*) and attenuation correction were applied to patient studies.

Resolution

Resolution within sections parallel to the collimator face (section resolution) and resolution between these sections (depth resolution) were determined with line sources in air and in water. A line source filled with an aqueous solution of ^{201}Tl was positioned parallel to, and at different distances from, the collimator face. The values of a count profile through a reconstructed section were fitted to a Gaussian curve by the method of least-squares. The full width at half maximum (FWHM) of the Gaussian curve was used as the measure of resolution. Pixel sizes were 0.3 or 0.6 cm depending on the distance from the collimator.

Effects of Misalignment

Phantom studies were performed with a homogeneous cylinder (1,000 ml plastic bottle, diameter 9 cm) filled with an aqueous solution of technetium-99m. The long-axis of the phantom was tilted 0°, 12°, 20°, 30°, and 40° with respect to the axis of rotation. Pixel size was 0.6 cm. Variation in section image uniformity was studied in three reconstructed sections by means of count profile analysis and a normalized sum of squares distance (*32*). The latter provides a measure of the deviation between two images. One section was through the middle (central) and the other two through the opposite ends of the phantom (apical and basal).

Left Ventricular Phantom

Two perspex left ventricular phantoms were used. With a multichamber cardiac phantom approximately following the design of Mueller et al. (*33*), usually called the Iowa phantom, relative activity distributions were studied. A detailed description of the phantom is given in Figure 1.

All but the 24-ml chamber (E) of the Iowa phantom were filled with a standard solution obtained by adding 100 MBq ^{201}Tl to 700 ml water. An aliquot of this solution was diluted to 5% and was used to fill the central cavity (A). Four measurements were made with different activity levels in the 24-ml chamber (E): initially dilution of the standard solution to 0%, i.e., no activity, then dilutions to 25%, 50% and 75%, respectively. A 21-liter glass tank was positioned with its long side towards the collimator face and the phantom was placed in the tank a few centimeters to the left of the middle with a misalignment of 12° with respect to the axis of rotation in both a left anterior oblique (LAO) direction and a cranial direction. The 24-ml chamber (E) was orientated to simulate a defect extending from the anterior to the septum wall. The permanent 6-ml defect was thus in the posterior wall of the phantom. The tank was filled with water; no background activity was added. Pixel size was 0.6 cm and acquisition time 40 sec/projection.

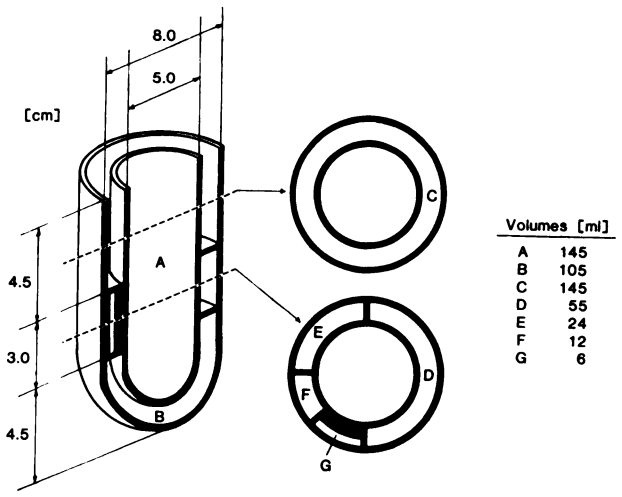

FIGURE 1
The Iowa phantom, which has an inner diameter of 5 cm and an outer of 8 cm; length from apex to base is 12 cm. The cavity chamber (A) contains 145 ml, the apex chamber (B) 105 ml, and the base chamber (C) 145 ml. The 3.0-cm midsection consists of five chambers that can simulate myocardial perfusion defects: one chamber extends 180° (D) and contains 55 ml, another (E) 90° and 24 ml, and a third (F) 45° and 12 ml. The fourth is divided into two parts, one part constitutes a permanent inner wall defect of 6 ml and the other, an outer wall chamber (G) containing 6 ml.

With a hollow cylindrical phantom, variation in activity distribution with depth and effects of misalignment were investigated. The phantom had an inner diameter of 5.2 cm, an outer diameter of 9.0 cm, and a length of 14.5 cm. The walls were filled with the standard solution and the cavity with a dilution to 5%. The phantom was orientated in the water tank in the same way as the Iowa phantom.

Section images parallel to the collimator face of nominal thickness, 1.2 cm, were reconstructed and studied with circumferential profile analysis (*34*) and regions of interest (ROIs). Circumferential profiles were generated with commercially available software (SPECT V06-TSX, Nuclear Diagnostic Co. Ltd., Stockholm, Sweden) for basal, central, and apical section images. ROIs were manually assigned to different regions of the image phantom wall—in the lateral, anterior, septum, and posterior wall. Their ratios were compared at varying depths.

Patients

Ten consecutive patients referred for routine tomographic myocardial ^{201}Tl imaging (SPECT) were studied. Informed consent was obtained. During maximum symptom-limited exercise on bicycle ergometer, ~80 MBq of ^{201}Tl was administered (*35*). In all patients, SPECT was performed first, beginning 10 min after injection of ^{201}Tl, and the method presented here ~45 min afterwards. (There was no possibility of randomizing the order of imaging in this study.)

In SPECT, clinical practice was followed and the gamma camera was rotated through 180°, from 45° left posterior oblique (LPO) to 45° RAO, and 32 projections were acquired. Each projection was registered for 40 sec, yielding a total acquisition time of 22 min. Pixel size was 0.5 cm. Short-axis section images of nominal thickness, 1.0 cm, were reconstructed.

In the method described, the slant-hole collimator was rotated through 360° and 64 projections were acquired. The gamma camera was positioned in a LAO 30° position with a 15° cranial tilt. Since the sensitivity of the slant-hole collimator was less than that used for SPECT acquisition, each projection image was registered for either 25 or 30 sec, yielding a total acquisition time of ~35 min. Pixel size was 0.6 cm. Section images parallel to the collimator face of nominal thickness, 1.2 cm, were reconstructed.

Comparison between section images was made using circumferential profile analysis and analysis of variance. For each patient, three different section images were studied (basal, central, and apical) and within each section image, four different regions (lateral, anterior, septum, and posterior). For each section, a mean difference circumferential profile was generated by averaging over all patients profile differences between the two methods.

RESULTS

Resolution

Section resolution in air using ^{201}Tl in terms of FWHM increased from 0.6 cm at 3 cm from the collimator face to 1.3 cm at 18 cm. In water, FWHM increased from 0.6 cm at 3 cm to 1.6 at 18 cm.

Depth resolution in air using ^{201}Tl in terms of FWHM increased from 2.1 cm at 3 cm from the collimator face to 4.9 cm at 18 cm and in water from 2.2 cm at 4 cm to 5.6 at 18 cm.

Effects of Misalignment

With no misalignment, count profiles of section images of the homogeneous cylindrical phantom showed a uniform activity distribution apart from a central deviation. This deviation from uniformity was due to distortion caused by high-pass filtration. Distortion occurs with the method described when the extension of the object perpendicular to the section is small compared to its extensions parallel to the section (*36*).

With misalignment, uniformity variation was present in basal section images: a decrease in activity was noticed in the side of the cylinder facing the collimator and an increase in the opposite side. As the misalignment angle became larger, this difference increased, until the misalignment angle was greater than the view angle and the difference decreased. In central section images, uniformity variation was negligible and in apical sections it was less pronounced than in basal section images. Hence, the effect of misalignment is dependent on the position of the section and is most pronounced in basal section images.

The normalized sum of squares distance between section images with and without misalignment increased with increasing misalignment angle and no improvement was achieved when short-axis section images were used. This was further confirmed by visual inspection. Hence, only section images parallel to the collimator face are considered in the following.

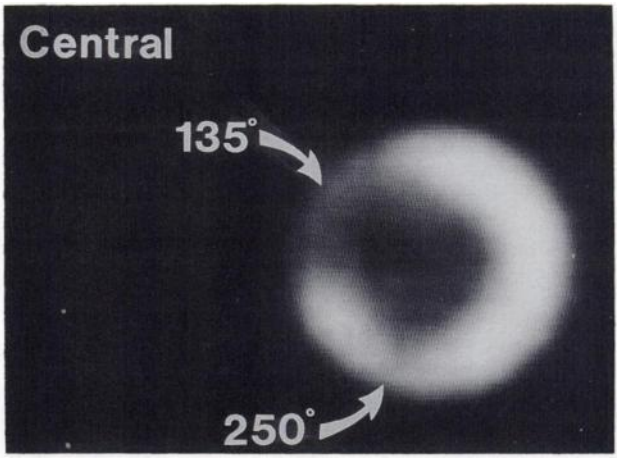

FIGURE 2
Section image (parallel to the collimator face) of the central section of the Iowa phantom with long axis orientated in 12° misalignment with respect to both the LAO and cranial direction. The 24-ml chamber (E) contained a dilution to 25% of the standard solution and was positioned in the anterio-septal region, while the permanent 6-ml inner wall defect was in the posterior region. Anterior is upwards, posterior downwards, the lateral wall is to the right and the septum is to the left.

Left Ventricular Phantom

In Figure 2, the central section image is shown of the misaligned Iowa phantom with a dilution to 25% of the standard solution in the 24-ml chamber (E). This decrease in activity is observed in the anteroseptal wall (135°) and the permanent inner wall defect is detected in the posterior wall (250°).

Circumferential profiles of the central section image are shown in Figure 3 for different dilutions of the standard in the 24-ml chamber (E). Profiles were normalized to the mean activity in the normal wall. Reconstructed defect activity levels do not accurately reflect real activity levels. Mean defect activity (nine values centered about 135°), was 35%, 42%, 60%, and 75% for dilutions to 0%, 25%, 50%, and 75% of the standard solution, respectively. For the hollow cylindrical phantom, mean "defect" activity was 106% centrally. The inner wall defect of the Iowa phantom caused the decrease in activity at 250° although the defect occupied only half of the wall thickness. Basally, mean activity in the defect region was below the expected 100% (47%, 52%, 63%, and 78%). Apically, depth resolution is superior and, therefore, the effect of misalignment was less, yielding a defect activity level closer to the expected 100% (75%, 80%, 90%, and 95%).

Patients

In Figure 4, section images of a myocardium in vivo are shown. Left ventricular orientation was LAO 32° and 21° cranial, as determined with the software used for SPECT reconstruction. Coronary angiography

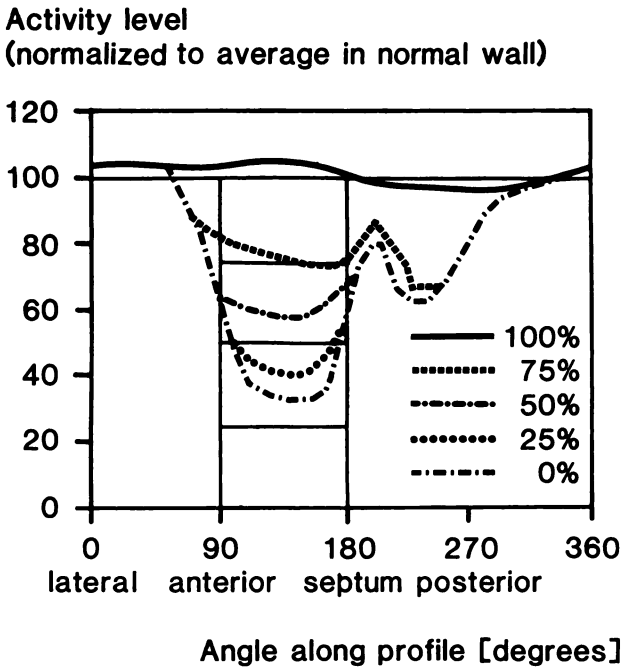

FIGURE 3
Central circumferential profiles of the Iowa phantom for different dilutions of the standard solution in the 24-ml chamber (E) and of the hollow cylindrical phantom. Real activity levels are shown in thin solid lines.

showed stenotic lesions in a diagonal branch of the left anterior descending coronary artery, in part of the left distal circumflex and in distal parts of the right coronary artery, indicating a probable reduction in perfusion in regions centered about approximately 0°, 135°, and 270°, respectively. In the method described, reduced perfusion is noticed about 135° and 270°, whereas in SPECT, reduced perfusion is noticed only about 270°. The 270° defect appears larger in SPECT. For the section images shown in Figure 5, left ventricular orientation was LAO 60° and 25° cranial. Thus, large misalignment was present. Centered about 330°, a region with reduced perfusion is detected with both methods.

The mean difference between circumferential profiles from the two methods for ten patients is shown in Figure 6. In every region, the difference was <25%; in basal profiles it was least and in apical greatest.

In an analysis of variance, a significant difference between the methods was found in the posterior and septal region ($p < 0.005$ and $p < 0.001$, respectively); normalized means of 0.90 and 0.90 for the method described, 0.82 and 1.00 for SPECT. In the anterior region, a significant difference between the methods was found anteriorly in basal ($p < 0.05$) and apical ($p < 0.01$) sections; normalized means of 1.08 and 1.06 for the method described, 1.17 and 0.96 for SPECT.

DISCUSSION

Missing coefficients in the Fourier domain form a volume shaped as a double cone, which has an axis of symmetry parallel to the axis of rotation. If the object imaged only changes slowly in this direction, distortion in the reconstructed sections will be moderate. The myocardium has such a geometry if alignment of the long-axis of the left ventricle is achieved. With misalignment, artifacts can be produced in the reconstructed section image. In our study, 12° misalignment of a hollow cylinder produced only small false defects in basal and apical section images. Section images of a homogeneous cylinder with one end resembling an apex (bottle), showed significant false defects in basal images for misalignment angles larger than 20°, but not in central or apical images.

Compared to other RSH methods, the angular sam-

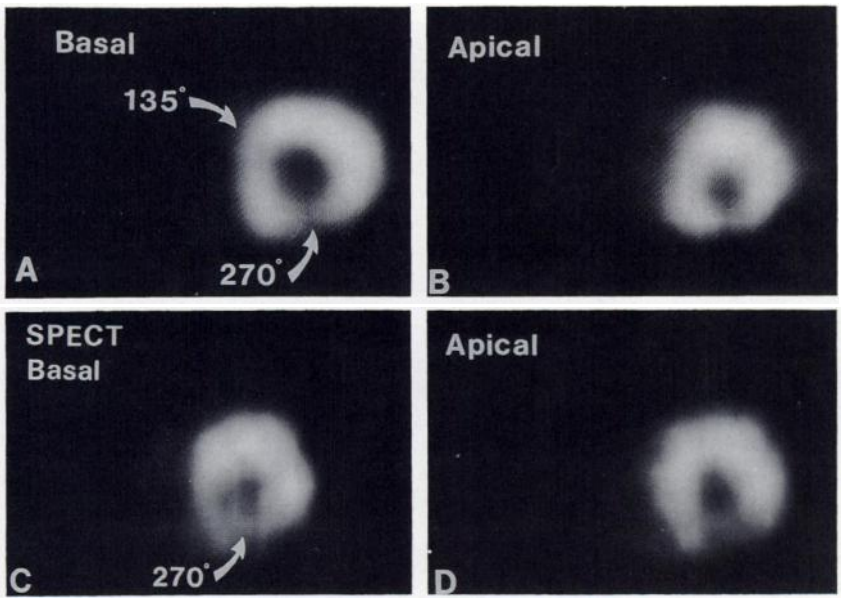

FIGURE 4
Section images of a myocardium in vivo with left ventricular orientation LAO 32° and 21° cranial. Coronary angiography showed stenotic lesions in a diagonal branch of the left anterior descending coronary artery, in part of the left distal circumflex, and in distal parts of the right coronary artery, indicating a reduced perfusion in regions centered around 0°, 135° and 270°, respectively. Anterior is upwards, posterior downwards, the lateral wall is to the right, and the septum to the left. (A–B) Method presented. Section images, parallel to the collimator face. Nominal section thickness 1.2 cm. Note a reduced perfusion in regions centered about 135° and 270°. (C–D) SPECT short-axis section images. Nominal section thickness is 1.0 cm. Note a reduced perfusion in a large region centered about 270°.

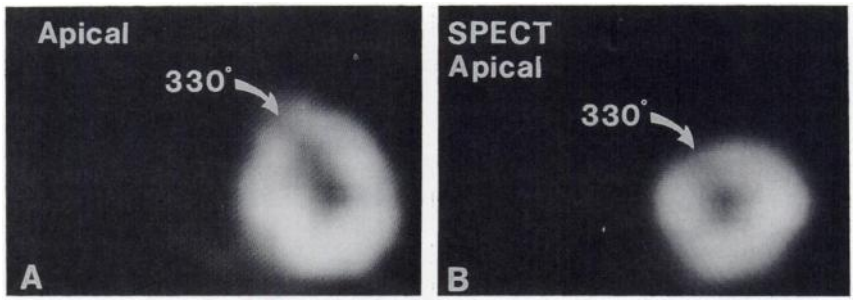

FIGURE 5
Section images of a myocardium in vivo with left ventricular orientation LAO 60° and 25° cranial. (A) Method presented. Section image, parallel to the collimator face. Nominal section thickness is 1.2 cm. Note a reduced perfusion in a fairly large region centered about 330°. (B) SPECT short-axis section image. Nominal section thickness is 1.0 cm. Note a reduced perfusion in the same region.

pling frequency is higher in the method described. On average, eight times as many projections are registered, resulting in a distortion-free image of details in the section. With a low angular sampling frequency, image distortion arises if the details do not have rotational symmetry about the axis of rotation. Tomographic imaging is thus limited to objects having circular cylinder symmetry.

Myocardial imaging with the method presented was performed in a LAO 30° position with a 15° cranial tilt. This orientation was a compromise between a short distance (5–8 cm) from myocardium to gamma camera and alignment of the left ventricle with respect to the axis of rotation. Mean misalignment for the ten patients in this study was +7° in the LAO direction and +4° in the cranial direction and, despite a misalignment in one of the patients of 30° in the LAO direction and 10° in the cranial direction (Fig. 5), the section images were still of some diagnostic value. However, with individual positioning of the gamma camera for each patient, large misalignments should be avoided. The orientation of the left ventricle can be estimated by first registering a left lateral planar image. If the camera is positioned according to the observed cranial angle and moved in the LAO direction, optimal alignment is achieved when a planar image of the ventricle is as circular as possible. The mean misalignment for the patients also show that Iowa phantom misalignment was exaggerated. With a smaller misalignment angle, reconstructed defect activity levels would be closer to the true levels.

No significant difference was found in the analysis of variance between the methods when data from all regions (lateral, anterior, septum, posterior), all section images (basal, central, apical), and patients were studied as a whole. However, studied separately, significant differences were found, essentially in the posterior and septal regions. The significant difference in the septal region was probably not only due to overcorrection for attenuation in SPECT, but also to the effects of misalignment in the method described. The significantly larger activity value in the posterior wall for the new method than for SPECT was probably due to a reduction in the effects of attenuation and scatter in the method presented. This indicates an improved certainty in the evaluation of perfusion defects in this region.

As a result of the short distance from myocardium to gamma camera, section resolution was better in the method described than in SPECT. Hence, the right ventricle was more often visible and the myocardial wall of the left ventricle was thinner. The noise level in the section images appeared lower, which was probably due to a reduction in the effects of scatter and attenuation, but can also be due to the limited depth resolution. Since SPECT was always performed first, some

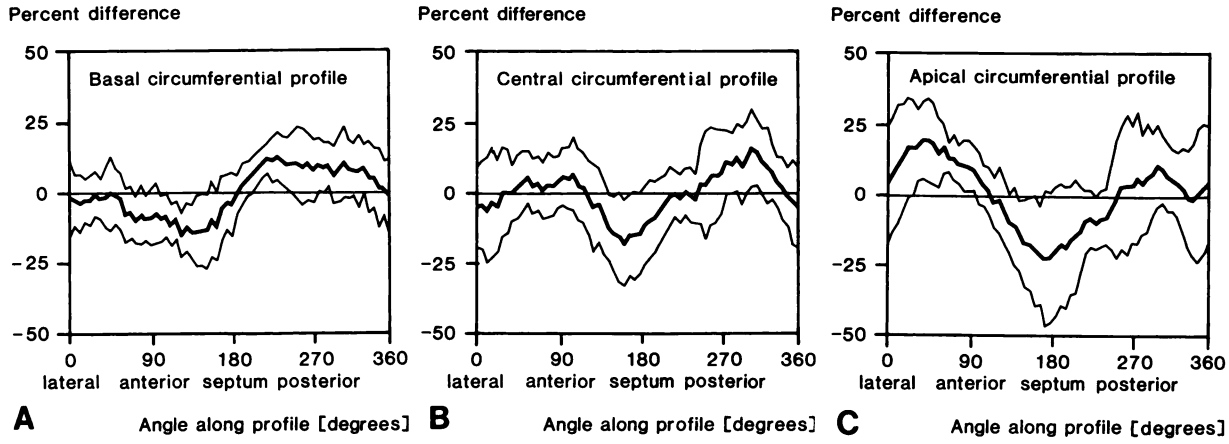

FIGURE 6
Mean difference between the method presented and SPECT circumferential profiles of the ten patients (thick solid line). Thin solid lines show ±1 s.d. (A) Basal, (B) central, and (C) apical.

of the differences observed between the method can presumably be explained by a redistribution of activity (*37*).

In conclusion, the difference between the method described and SPECT in myocardial imaging was relatively small as indicated in the analysis of variance and the mean difference circumferential profiles. Disadvantages of the method are the comparatively poor depth resolution and the effects of misalignment, which occur if the orientation of the left ventricle significantly deviates from the axis of rotation. However, misalignment should not be a problem if acquisition is performed in a direction of 30° LAO and 15° cranial or if left ventricular orientation is determined for each patient using the method described. Advantages of the method for tomographic ^{201}Tl myocardial imaging include a comparatively high section resolution, a distortion-free image of the section, a reduction in the effects of scatter and attenuation in mainly the posterior wall, and a possibility of performing tomography in intensive care units using a standard portable camera and a RSH collimator.

ACKNOWLEDGMENTS

This work was supported by grants from the Swedish National Board for Technical Development, Stockholm (project No. 83-04086P) and the Swedish Association Against Heart and Lung Diseases.

REFERENCES

1. Gerson MG, Thomas SR, van Heertum RL. Tomographic myocardial perfusion imaging. In: Gerson MG, ed. *Cardiac nuclear medicine.* New York: McGraw Hill-Book Company; 1987:25–52.
2. Budinger TF. Three-dimensional imaging of the myocardium with isotopes. In: Harrison CD, Sandler H, Miller HA, eds. *Cardiovascular imaging and image processing.* Palos Verdes, CA: Society Photo-Optical Instrumentation Engineers; 1975:263–271.
3. Holman BL, Hill TC, Wynne J, Lovett RD, Zimmerman RE, Smith EM. Single-photon transaxial emission computed tomography of the heart in normal subjects and in patients with infarction. *J Nucl Med* 1979; 20:736–740.
4. Tamaki N, Mukai T, Ishii Y, et al. Comparative study of thallium emission myocardial tomography with 180° and 360° data collection. *J Nucl Med* 1982; 23:661–666.
5. Holman BL, Idoine JD, Sos TA, Tancrell R, DeMeester G. Tomographic scintigraphy of regional myocardial perfusion. *J Nucl Med* 1977; 18:764–769.
6. Rogers WL, Koral KF, Mayans R, et al. Coded-aperture imaging of the heart. *J Nucl Med* 1980; 21:371–378.
7. Vogel RA, Kirch D, LeFree M, Steele P. A new method of multiplanar emission tomography using a seven-pinhole collimator and an Anger scintillation camera. *J Nucl Med* 1978; 19:648–654.
8. Williams DL, Ritchie JL, Harp GD, Caldwell JH, Hamilton GW. In vivo stimulation of thallium-201 myocardial scintigraphy by seven-pinhole emission tomography. *J Nucl Med* 1980; 21:821–828.
9. Gottschalk SC, Smith KA, Wake RH. Tomographic reconstructions with rotating slant-hole and seven-pinhole collimators on an Anger gamma camera phantom and clinical studies. In: Paras P, Eikman EA, eds. *Emission computed tomography: the single photon approach.* Rockville, MD: HHS Publication FDA 81-8177; 1981:105–128.
10. Nalcioglu O, Morton ME, Milne N. Computerized longitudinal tomography (CLT) with a bilateral collimator. *IEEE Trans Nucl Sci* 1980; 27:430–434.
11. Ratib O, Henze E, Hoffman E, Phelps ME, Schelbert HR. Performance of the rotating slant-hole collimator for the detection of myocardial perfusion abnormalities. *J Nucl Med* 1982; 23:34–41.
12. Chang W, Lin SL, Henkin RE. A new collimator for cardiac tomography: the quadrant slant-hole collimator. *J Nucl Med* 1982; 23:830–835.
13. Dale S, Bone D. Tomography using a rotating slant-hole collimator and a large number of projections. *J Nucl Med* 1990; 31:1675–1681.
14. Dale S, Edholm PE, Hellström LG, Larsson S. Ectomography—a tomographic method for gamma camera imaging. *Phys Med Biol* 1985; 30:1237–1249.
15. Edholm P, Granlund G, Knutsson H, Petersson C. Ectomography—a new radiographic method for reproducing a selected slice of varying thickness. *Acta Radiol Diagn* 1980; 21:433–442.
16. Knutsson HE, Edholm P, Granlund GH, Petersson CU. Ectomography—a new radiographic reconstruction method. I. Theory and error estimates. *IEEE Trans Biomed Eng* 1980; 27:640–648.
17. Chiu MY, Barrett HH, Simpson RG, Chou C, Arendt JW, Gindi GR. Three-dimensional radiographic imaging with a restricted view angle. *J Opt Soc Am* 1979; 69:1323–1333.
18. Buddinger TF. Physical attributes of single-photon tomography. *J Nucl Med* 1980; 21:579–592.
19. Chang W, Lin SL, Henkin RE. Long-axis alignment in collimator tomography of the heart [Abstract]. *J Nucl Med* 1981; 22:P66.
20. Ratib O, Henze E, Schelbert HR. Effect of positioning on detection of myocardial perfusion abnormalities by the rotating slant-hole collimator [Abstact]. *J Nucl Med* 1981; 22:P66.
21. Chang W, Henkin RE. Performance of the rotating slant-hole collimator for the detection of myocardial perfusion abnormalities. *J Nucl Med* 1982; 23:547.
22. Rizi HR, Kline RC, Thrall JH, et al. Thallium-201 myocardial scintigraphy: a critical comparison of seven-pinhole tomography and conventional planar imaging. *J Nucl Med* 1981; 22:493–499.
23. Hasegawa B, Kirch D, Stern D, et al. Single-photon emission tomography with a 12-pinhole collimator. *J Nucl Med* 1982; 23:606–612.
24. Koral FK, Nolder C, Ciliax G, Rogers WL, Keyes Jr JW. Simulated ECT of the left ventricle using rotating slant-hole collimator and two camera positions. *J Nucl Med* 1984; 25:343–351.
25. Mills JA, Flint J, Taylor DN, Delchar T, McIntosh JA, Pilcher J. Thallium-201 scintigraphy for ischemic heart disease and infarct detection: comparison of rotating slant-hole tomography and planar imaging. *Br J Radiol* 1985; 58:625–634.
26. Starling MR, Dehmer GJ, Lancaster JL, et al. Segmental coronary artery disease: detection by rotating slant-hole collimator tomography and planar thallium-201 myocardial scintigraphy. *Radiology* 1985; 157:231–237.
27. Lancaster JL, Starling MR, Kopp DT, Lasher JC, Blumhardt R. Effect of errors in reangulation on planar and tomographic thallium-201 washout profile curves. *J Nucl Med* 1985; 26:1445–1455.
28. Mills JA, Delchar TA. Origin of the false defect in longitudinal emission computed tomography of the left ventricle. *Phys*

Med Biol 1988; 33:969–973.
29. Shepp LA, Logan BF. The Fourier reconstruction of a head section. *IEEE Trans Nucl Sci* 1974; 21:21–43.
30. Chesler DA, Riederer SJ. Ripple suppression during reconstruction in transverse tomography. *Phys Med Biol* 1975; 20:632–636.
31. Grant DG. Tomosynthesis: a three-dimensional radiographic imaging technique. *IEEE Trans Biomed Eng* 1972; 19:20–28.
32. Rowland SW. Computer implementation of image reconstruction formulas. In: Herman GT, ed. *Image reconstruction from projections. Implementation and applications.* Heidelberg: Springer Verlag; 1979:9–79.
33. Mueller TM, Marcus ML, Ehrhardt JC, Chaudhuri T, Aboboud FM. Limitations of thallium-201 myocardial perfusion scintigrams. *Circulation* 1976; 54:640–646.
34. Burow RD, Pond M, Schafer AW, Becker L. "Circumferential profiles: " a new method for computer analysis of thallium-201 myocardial perfusion images. *J Nucl Med* 1979; 20:771–777.
35. Bone D, Holmgren A, Svane B. Thallium tomography in the detection of myocardial perfusion defects. *Acta Med Scand Suppl* 1984; 694:109–119.
36. Dale S, Edholm P. Inherent limitations in ectomography. *IEEE Trans Med Imag* 1988; 7:165–172.
37. Schwartz JS, Ponto R, Carlyle P, Forstrom L, Cohn JN. Early redistribution of thallium-201 after temporary ischemia. *Circulation* 1978; 57:332–335.

EDITORIAL: Limited-Angle Tomography for the Nineties

This issue of *The Journal of Nuclear Medicine* includes two articles (*1*,*2*) on what many would regard as an outmoded technique, limited-angle tomography with a rotating slant-hole collimator (RSH). Is there a role for such methods in the age of sophisticated tomographic techniques such as SPECT and PET? Before attempting to answer that question, let us take a brief look at the historical and mathematical background.

HISTORICAL BACKGROUND

Tomography is one of the oldest ideas in radiology. The basic concept of selecting a plane of interest by relative motion of source and detector is apparently due to Bocage in 1921 (*3*), but the first practical demonstration was made by Vallebona in Italy in 1930 (*4*). Many ingenious variations on this theme were developed over the next half century, and many different names, such as planigraphy, stratigraphy and laminography, were applied. We shall refer to all of these methods collectively as *classical tomography*. The common ingredient in these methods is that they obtain depth discrimination by parallax.

Received Jul. 5, 1990; acceptedJul. 5, 1990.
For reprints contact: Harrison H. Barrett, PhD, Dept. of Radiology and Optical Sciences Center, University of Arizona, Tucson, AZ 85724

The advent of computed tomography in the seventies essentially led to the demise of classical tomography in diagnostic radiology (though a few clinical applications remain). Computed tomography (CT) is superior because it completely eliminates image information from planes other than the desired one (for the simple reason that the radiation is confined to that plane). By contrast, the classical methods merely blur the undesired planes, as in a microscope, but do not eliminate them. The out-of-focus structures reduce the contrast in the plane of interest and interfere with diagnosis. In this discussion, we shall use the terms computed tomography and classical tomography in a broad sense: classical tomography is any method that blurs undesired planes, while computed tomography eliminates them. It is clear that CT is preferred over classical methods in diagnostic radiology today.

In nuclear medicine, the evolution of tomography took a rather different course. The earliest tomographic system for nuclear medicine, introduced by Kuhl and Edwards (*5*) in 1963, was in fact a CT system (SPECT, in particular). Classical motion tomography was introduced to the field a little later, with the advent of the Anger tomoscanner (*6*) in 1966 and the Vanderbilt tomoscanner (*7*) in 1969. Many other methods soon followed, among them the RSH collimator, the seven-pinhole aperture, and a wide variety of coded apertures. For a good review of this field, see Koral (*8*).

MATHEMATICAL BACKGROUND

To this point we have not introduced the term *limited-angle tomography*. One definition of this term is by exclusion: a limited-angle tomographic system is one in which the data collection does not span the full range of projection angles needed for accurate image reconstruction. To apply this definition, we must of course specify the required full angular range. For parallel-beam projections confined to a plane, as in the first-generation CT scanners, the full angular range in projection angle is 180°. The easiest way to see this is to appeal to the projection-slice theorem, which states that each projection gives information about the Fourier transform of the object along one line through the center of the two-dimensional (2-D) Fourier plane. If projections are collected for all angles over a range of 180°, these lines sweep over the entire 2-D Fourier plane. Since an object is uniquely specified by its Fourier transform, it can thus be reconstructed unambiguously from projections over a con-